Rapid Communications

Origin of sawtooth domain walls in ferroelectrics

J. Zhang,[1] Y.-J. Wang,[2] J. Liu,[3] J. Xu,[1] D. Wang,[1,*] L. Wang,[4] X.-L. Ma,[2] C.-L. Jia,[1,5] and L. Bellaiche[6]

[1]*School of Microelectronics and State Key Laboratory for Mechanical Behavior of Materials, Xi'an Jiaotong University, Xi'an 710049, China*

[2]*Shenyang National Laboratory for Materials Science, Institute of Metal Research, Chinese Academy of Sciences, Wenhua Road 72, 110016 Shenyang, China*

[3]*State Key Laboratory for Mechanical Behavior of Materials, School of Materials Science and Engineering, Xi'an Jiaotong University, Xi'an 710049, China*

[4]*Electronic Materials Research Laboratory, School of Electronic Science and Engineering, Xi'an Jiaotong University, Xi'an 710049, China*

[5]*Ernst Ruska-Center for Microscopy and Spectroscopy with Electrons, Forschungszentrum Jülich GmbH, 52425 Jülich, Germany*

[6]*Department of Physics and Institute for Nanoscience and Engineering, University of Arkansas, Fayetteville, Arkansas 72701, USA*

(Received 29 May 2019; revised manuscript received 12 October 2019; accepted 7 February 2020; published 25 February 2020)

Domains and domain walls are among the key factors that determine the performance of ferroelectric materials. In recent years, a unique type of domain walls, i.e., the sawtooth-shaped domain walls, has been observed in $BiFeO_3$ and $PbTiO_3$. Here, we build a minimal model to reveal the origin of these sawtooth-shaped domain walls. Incorporating this model into Monte Carlo simulations shows that (i) the competition between the long-range Coulomb interaction (due to bound charges) and short-range interaction (due to opposite dipoles) is responsible for the formation of these peculiar domain walls and (ii) their relative strength is critical in determining the periodicity of these sawtooth-shaped domain walls. Necessary conditions to form such domain walls are also discussed.

DOI: 10.1103/PhysRevB.101.060103

Domains, which are typical regions with aligned magnetic moments or electric dipoles, can largely influence phase transitions and physical properties of magnetic or ferroelectric materials. For ferroelectrics, attention has been paid to investigate domains' characteristics and properties [1–5]. When changing from the paraelectric to the ferroelectric phase, the symmetry of equivalent dipole directions is broken, giving rise to regions with different polarization directions while each region has a preferred polarization direction. Ferroelectric domain walls have received extensive attention due to various novel phenomena, including stable patterns on the nanometer scale. Domains have been carefully analyzed to reveal the correlation between the micro/nanoscale structure and the properties of the materials [6–9], often through high-resolution x-ray diffraction technique [10,11]. For instance, polarization switching is a critical link between domains and material performance [12–17]. In bulk ferroelectrics, the domain structure, closely related to phase structure, was thoroughly discussed along with domain size and morphology. On an even smaller scale, polar nanoregions as a special type of domains have also been discussed [18–23].

Recently, charged domain walls have attracted much investigation [24,25]. The charged domain wall is an ultrathin (usually nanoscale) interface between two domains, which carries bound charges due to the abrupt change of the normal component of spontaneous polarization on the interface, causing discontinuity of the polarization. The head-to-head configuration in adjacent domains leads to a positive charge. Tail-to-tail domain walls are charged negatively. The head-to-tail configurations can also carry bound charges, with their sign depending on the orientation of the wall. Due to the competition between the electrostatic energy (aligned dipoles usually have smaller electrostatic energy) and the domain wall energy (the extra energy necessary to have domains), domains can have very different morphologies, such as rhombohedral, orthorhombic, and tetragonal domains [26]. However, it was still quite surprising when sawtooth-shaped 180° domain walls were observed in multiferroic $BiFeO_3$ (BFO) [see Fig. 4(a) of Ref. [27]], which has a spontaneous polarization along the pseudocubic $\langle 111\rangle_c$ direction (that can be as large as 90–95 $\mu C/cm^2$ [28]) and a high Curie temperature ($T_C = 820\,^{\circ}C$) [29–31]. Note that the $BiFeO_3$ sample of Ref. [27] was cut along $\langle \bar{1}\bar{1}0\rangle$ and $\langle 1\bar{1}0\rangle$ while extending 55 nm vertically when high-resolution transmission electron microscopy (HRTEM) images were taken. More recently, Zou *et al.* [32] also observed serrated 180° domain walls in $PbTiO_3$ (PTO) thin films prepared by pulsed laser deposition. This PTO thin film was 100 nm thick and epitaxially grown on a (100)-oriented single crystal $SrTiO_3$ substrate (see Figs. 2 and 4 of Ref. [32]). These observations indicate that sawtooth-shaped domain walls constitute a general phenomenon in ferroelectrics, not limited to multiferroics or magnetic materials [33,34]. The bound charge on domain walls can be quite large (for BFO, the bound charge is estimated to be $1.64\,|e_0|$, where e_0 is the electron charge [35]), which can strongly affect the conductivity of the material by attracting free charge carriers, making them good candidates for domain wall electronics [36–38]. Recent

*dawei.wang@xjtu.edu.cn

 ©2020 American Physical Society

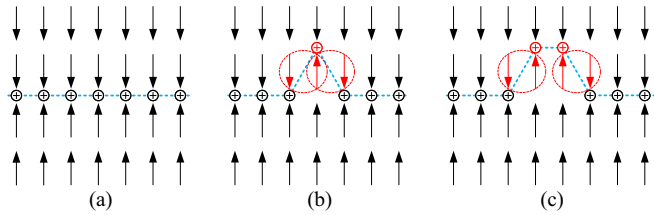

FIG. 1. Schematic drawing of dipoles and bound charges. (a) The black arrows represent dipoles, while the blue line depicts the 180° domain wall. The symbol "⊕" between dipoles represents bound charges formed by head-to-head dipoles. (b) When a dipole is reversed, the domain wall and the position of one bound charge change accordingly, and two pairs of opposite electric dipole pairs are generated at the left and right sides of the reversed dipole. (c) Another configuration can also involve two pairs of opposite dipoles.

research also show that negative capacitance is also closely related to dipole patterns and domain structures [39,40].

While charged domain walls have been known for a long time [41] and different aspects had been investigated including their conductivity [24,25,36,42,43], their influence on other dipoles and enhancement of material performance [44,45], and their dynamics of the charged domain wall and interaction with electric field [46–50], we are not aware of theoretical work to explain the formation mechanism of the sawtooth-shaped charged domain walls in ferroelectric materials. In this work, we explore possible causes of this unique phenomenon of sawtooth-shaped domain walls, finding that the long-range Coulomb interaction between bound charges and the short-range interaction between opposite dipole pairs are adequate to reproduce such peculiar domain walls. As a matter of fact, in order to understand the sawtooth domain walls, we propose a minimal model with just short-range interaction between opposite dipoles and long-range Coulomb interaction due to bound charges arising from the head-to-head dipoles, and following a similar approach as the effective Hamiltonian [51–56] to simulate two-dimensional (2D) and three-dimensional (3D) ferroelectric materials. We assume that (i) electric dipoles of opposite directions already exist in the system, and (ii) a boundary exists between the two groups of opposite dipoles (see Fig. 1). As bound charges accumulate on the boundary, their positions can be used as dynamic variables in simulations while the number of bound charges is fixed, which determines both the Coulomb energy and the short-range interaction as Fig. 1 shows. Therefore, the total energy for the system is given by

$$E^{\text{tot}} = E^{\text{cc}}(\{\boldsymbol{r}_i\}) + E^{\text{short}}(\{\boldsymbol{r}_i\}), \tag{1}$$

where $\boldsymbol{r}_i$ is the position of the ith bound charge. E^{short} is the short-range energy when neighboring ions have relative shifts [51]. For the 2D case shown in Fig. 1, the short-range interaction on the domain wall can be expressed as $E^{\text{short}} = JN$, where $J > 0$ is the additional energy associated with opposite neighboring dipoles and N (depending on $\{\boldsymbol{r}_i\}$) is the number of opposite dipole pairs. $E^{\text{cc}} = \frac{1}{2}\sum_{i,j} Z^2/\varepsilon_r|\boldsymbol{r}_i - \boldsymbol{r}_j|$ is the long-range charge-charge Coulomb energy, where Z is the bound charge, ε_r is the relative permittivity, and the energy

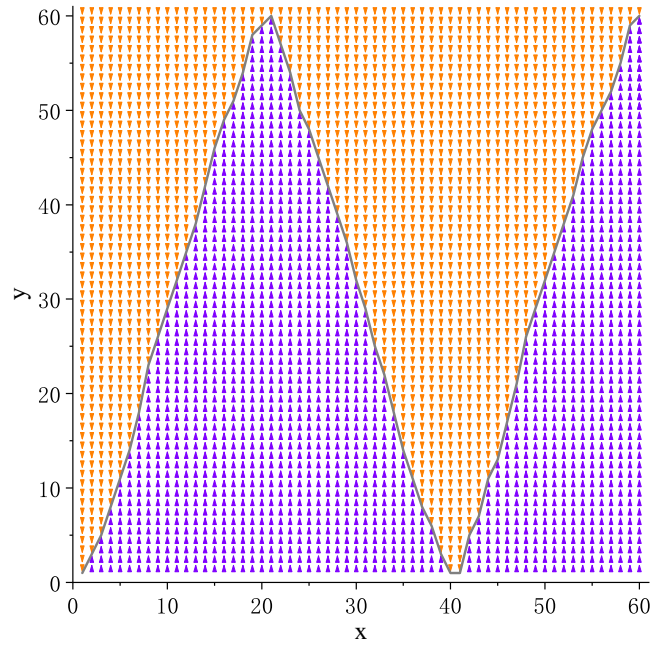

FIG. 2. Sawtooth-shaped domain wall in a 60 × 60 2D lattice.

unit is Hartree. Since the sawtooth domain wall induces bound charges and opposite dipole pairs, E^{tot} can also be regarded as the formation energy of the domain wall. For simplicity, we use the energy of Fig. 1(a) as the reference energy E_0, implicitly subtracting E_0 from E^{tot} hereafter. It shall be emphasized that the proposed energy terms constitute a minimal model that, as we will show, demonstrate why sawtooth domain wall arises. More sophisticated phenomenological models will be discussed in the Supplemental Material [57]. We note that the total energy in Eq. (1) is essentially a functional depending on the configuration of bound charges.

Using the total energy of Eq. (1), Monte Carlo (MC) simulations are employed to find the equilibrium domain wall morphology. During the simulation, the positions of the bound charges ($\boldsymbol{r}_i$) are tracked and changed to minimize the free energy. In each MC simulation at 300 K, we perform 320 000 sweeps of all the $\boldsymbol{r}_i$. We will first show the simulation results and then discuss how the parameters (J and Z) can affect the morphology. For the 2D case, we use a 60 × 60 supercell to mimic a planar sample. The bound charge is chosen as $Z = 1.16|e_0|$, which is an approximate estimation from the $R3c$ phase $BiFeO_3$ [35], while the short-range interaction parameter is taken to be $J = 0.005\,86$ Hartree (1 Hartree = 27.2 eV). The relative permittivity is $\varepsilon_r = 7.164$ which renders a Coulomb energy of $Z^2/\varepsilon_r a_0$, where a_0 is the lattice constant. We note J and ε_r can be inferred from the parameters used in the effective Hamiltonian for BFO [31,58–60] and the value of J is compatible with the formation energy calculation of domain walls [61–63]. As we will see, the parameter $\alpha = J/(Z^2/\varepsilon_r a_0)$ will largely determine the configuration. Figure 2 displays a typical 2D simulation result, in which the sawtooth domain walls can be clearly seen. The domain walls have an inclination of 71.47° (the inclination will be determined by energy analysis) and can steadily exist for 200 000 MC sweeps. For the 3D case, we use the Ewald method [64],

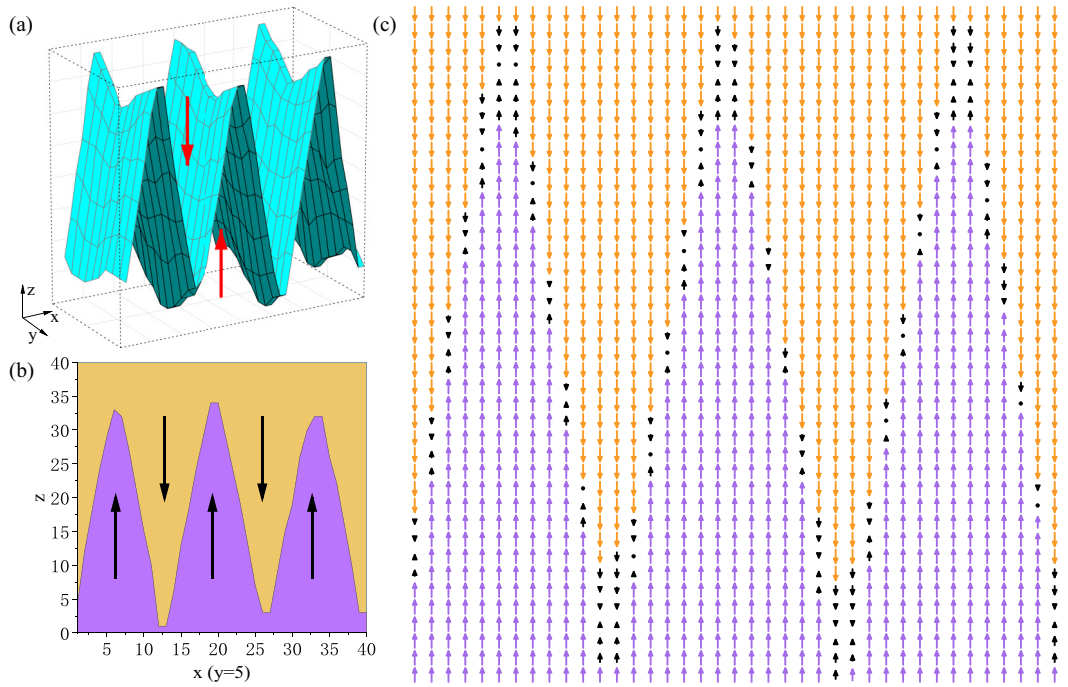

FIG. 3. Sawtooth-shaped domain wall in 3D using a $40 \times 10 \times 40$ supercell. (a) It contains a series of conical depressions and bulges. (b) The cross section at $y = 5$ shows a jagged domain wall. (c) The projection of the dipoles on the x-z plane shows reduced dipoles (black arrows) due to the average of dipoles over different y sections.

which naturally models the periodic boundary conditions of the supercell, to accelerate the evaluation of the Coulomb energy. The short-range interaction is treated similarly as in 2D, except that four nearest neighbors need to be considered instead of two. Considering the experimental situation (e.g., PTO on STO where ferroelectric regions are separated by nonferroelectric ones), we do not assume bound charges exist on the top-bottom boundary. Moreover, for the 2D case, a direct summation of Coulomb energy for nonperiodic boundary conditions is used for an easier simulation program and avoiding complications with the Ewald method for the 2D case [65].

Using a $40 \times 10 \times 40$ supercell, we carry out 320 000 sweeps of MC simulation at 300 K, and the resulting domain wall is shown in Fig. 3(a). Figure 3(b) shows the cross section at $y = 5$ where a triangular sawtooth domain wall can be clearly seen. To compare to experimental HRTEM images, we have also projected the dipoles along the y direction, averaging along each column, which results in Fig. 3(c). This figure not only demonstrates the sawtooth domain walls, but can also explain the smaller dipoles separating the two domains as observed in experiment [see Fig. 5(a) of Ref. [27]].

As we have seen, this model, which involves only Coulomb and short-range interactions, is adequate to reproduce the sawtooth domain walls. With this model, it is also possible to reveal and understand how Z and J can affect the domain wall morphology. To simplify the analysis, we use the 2D case as an example and only consider triangular sawtooth domain walls with different inclinations (see Fig. 4). The length of the domain wall can be formally defined as (in units of a_0) $\sum_i \sqrt{(x_{i+1} - x_i)^2 + (y_{i+1} - y_i)^2}$. As shown in Fig. 4, $x_{i+1} - x_i = 1$, therefore the length is given by $\sum_i \sqrt{1 + (y_{i+1} - y_i)^2}$. Because the bound charge can only shift in the up and down directions, it can be further simplified to its y component as

$$l = \sum_i |y_{i+1} - y_i|, \tag{2}$$

which can unambiguously determine the triangular domain wall. One advantage of this definition is that the short-range energy is directly proportional to l [see Fig. 5(a)], i.e., $E^{\text{short}} = Jl$. The Coulomb energy also depends on l as $E^{\text{cc}} = E^{\text{cc}}(l) - E_0^{\text{cc}}$ where $E_0^{\text{cc}} = Z^2\gamma/a_0$ (in units of hartree) and γ is a

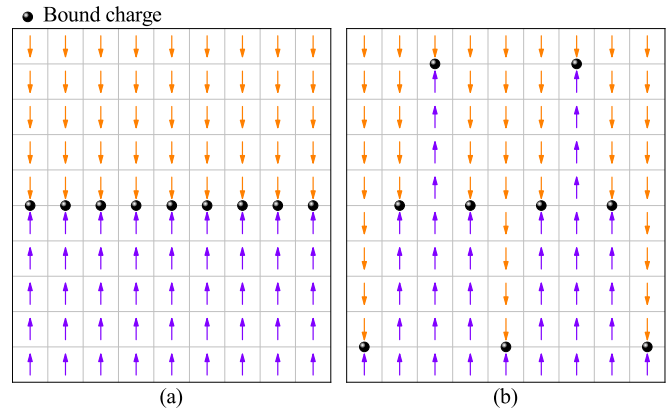

FIG. 4. Schematic diagram of the domain wall shape changing with its length. (a) In this case ($l = 0, T = \infty$), the length of the domain wall is zero, and it has the minimal short-range interaction and maximal Coulomb interaction. (b) As the length becomes larger ($l = 32a_0$, $T = 5a_0$), the domain wall appears inclined. The Coulomb interaction decreases while the short-range interaction increases.

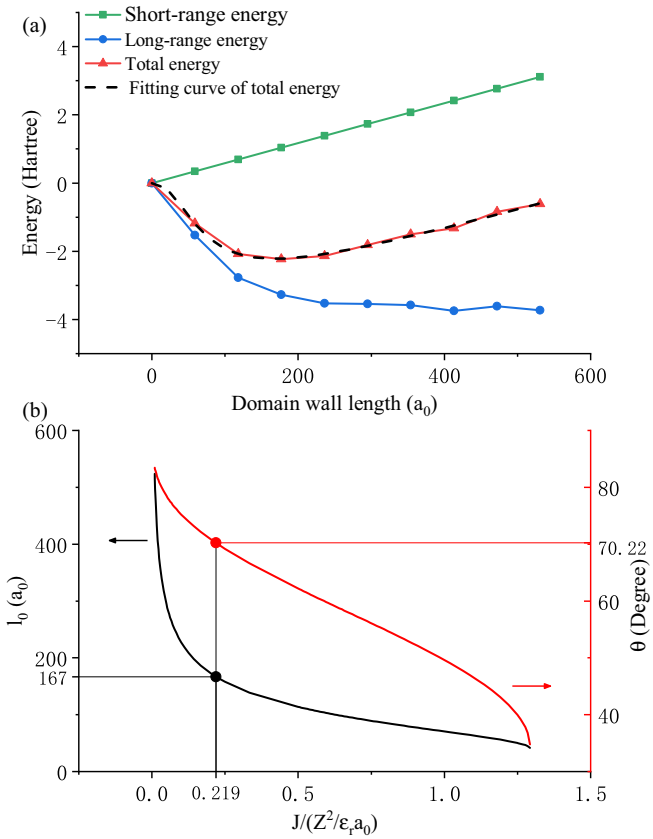

FIG. 5. (a) The constituent energies versus the length of the domain wall. The short-range interaction increases linearly, while the Coulomb interaction decreases (symbols are from numerical computations). (b) The stabilized domain wall length (l_0, black line) and inclination (θ, red line) versus $J/(Z^2/\varepsilon_r a_0)$.

constant calculated according to the charge positions shown in Fig. 4(a).

As l increases, the domain wall becomes sharper (i.e., the inclination increases) [see Fig. 4(b)]. Given a domain wall length, we can numerically calculate its constituent energies, which are shown as symbols in Fig. 5. It can be seen that the Coulomb energy and the short-range interaction energy show opposite trends with the length of domain wall. The short-range interaction increases with l, since larger l means more opposite dipole pairs. The Coulomb energy decreases with l due to the increase of bound charge distance.

To proceed further, we propose to use $E^{\rm cc} = \frac{Z^2\gamma}{a_0\varepsilon_r}(\frac{1+bl^2}{1+al^2} - 1)$ to describe how the Coulomb energy changes with l, where $\gamma = 220.8$ for a 60×60 simulation box. As a matter of fact, this expression can be used to fit the numerically computed Coulomb energy in Fig. 5, giving $a = 1.99 \times 10^{-4}$ and $b = 7.18 \times 10^{-5}$. The total energy is then given by

$$E^{\rm tot} = Jl + \frac{Z^2\gamma}{\varepsilon_r a_0}\left(\frac{1+bl^2}{1+al^2} - 1\right), \tag{3}$$

which can be derived by first considering the decrease of the long-range energy with l [the blue line with solid circles in Fig. 5(a)]. The variation of the total energy with l is also shown in Fig. 5(a). The equilibrium domain wall length l_0 can be found by minimizing the total energy with respect to l, and its dependence on $J/(Z^2/\varepsilon_r a_0)$ is shown in Fig. 5(b). This result indicates that the parameter $\alpha \equiv J/(Z^2/\varepsilon_r a_0)$ is crucial for determining the domain morphology (which is independent of their absolute value) and larger α tends to bind the bound charges closer to each other.

In the simulations that generate Figs. 2 and 3, $\alpha = 0.22$ is used. The resulting domain wall length and sawtooth period are consistent with the theoretical estimation. In numerically obtaining l_0 for Fig. 5(b), we find that when $\alpha > 1.29$, no solution can be found for l_0, which is consistent with our numerical findings (not shown here) that arbitrarily chosen J and Z cannot support the existence of such domain walls.

It shall be noted that the precondition for the above analysis is that triangular domain walls already exist. The constraint of $\alpha < 1.29$ can be understood by estimating the two energies of the configuration shown in Fig. 4(b). Assuming that two neighboring bound charges are shifted by y vertically, the short-range interaction is NJy ($N = 60$ for the 60×60 simulation box), while the Coulomb energy pertaining to this configuration is the horizontal line of bound charges [Fig. 4(a)] tilted by an angle of θ ($\tan\theta = y$), giving the energy of $(Z^2\gamma/\varepsilon_r a_0)(1/\sqrt{1+y^2} - 1)$. Since the Coulomb energy and the short-range interaction energy shall balance each other (not that one overwhelms the other) and reduce the total energy, therefore $NJy + Z^2\gamma/\varepsilon_r a_0(1/\sqrt{1+y^2} - 1) < 0$ is necessary, resulting in $\alpha < \gamma(1 - 1/\sqrt{1+y^2})/(Ny) \leqslant 1.10$ for $N = 60$, where the maximum is reached when $y = 1.27$. Since the Coulomb energy in the triangular case shall be larger than this value as the bound charges are closer, the final value of α shall be smaller than 1.10.

In fact, a more stringent constraint can be obtained with Fig. 4(a) as the initial configuration and consider only one bound charge (the first one from the left) is shifted upward by y, which satisfies $Jy + (Z^2/\varepsilon_r a_0)\sum_{n=1}^{N-1}(1/\sqrt{n^2+y^2} - 1/n) < 0$ or $\alpha < \sum_{n=1}^{N-1}(1/n - 1/\sqrt{n^2+y^2})/y \leqslant 0.42$ where the maximum is reached when $y = 1.7$. This result further constrains the parameters that can form sawtooth domain walls, indicating that there is an upper bound for α to make the sawtooth domain walls possible. This constraint, which is necessary to form sawtooth domain walls, is also verified using MC simulation. For the 3D case, using the parameters chosen for BFO, we found when $\alpha < 0.806$, the sawtooth domain wall is possible.

In addition to the constraint on α, it was pointed out that 180° domain occurs when no (or very small) epitaxial strain is applied from the substrate, while 90° or other domain patterns are expected with larger values [32,66,67]. This can be understood with the strain-dipole coupling [51], where the dipoles experience extra energy from strain, which likely makes their flipping more difficult comparing to a partial rotation of 90°, effectively increasing the J parameter. In addition, similar to magnetic domain walls [68], dislocation, impurity, and defect can also hinder domain wall growth.

Since charged domain walls can be compensated by free charge carriers [44,47], the tendency of the wall to be inclined is reduced as the Coulomb interaction is reduced (α becomes larger). Depending on the value of J, the sawtooth domain could still exist if J is small enough. On the other hand, we need to note that charged domain walls are not always

compensated by free carrier, such as the hybrid perovskite materials [69].

In this work we have used bound charge as the fundamental variable to construct the energy functional. If one is interested to employ dipole ($\boldsymbol{P}$) as the variable and construct the energy functional accordingly, our results indicate that $\nabla \cdot \boldsymbol{P}$ will be the key ingredient of such a functional. Since head-to-head (or tail-to-tail) dipole configurations are high-energy excitations often associated with extrinsic factors [70], other energy terms with $\boldsymbol{P}$ are less important than the $\nabla \cdot \boldsymbol{P}$ terms for sawtooth domain walls, except for providing a background. We therefore believe the use of bound charge as the fundamental variable is the right choice since $-\nabla \cdot \boldsymbol{P}$ is nothing but the bound charge. Such energy term with bound charge is known as the *stray field* energy in micromagnetic simulations [71]. We finally note that there is a strong parallel between the ferroelectric and magnetic dipoles and a lot can be learned from previous investigations in magnetism for ferroelectrics [72].

In summary, we have built a minimal model to reveal the origin of the sawtooth-shaped domain walls observed in ferroelectric materials. Our model-based MC simulations show that the competition between the long-range Coulomb energy from bound charges and the short-range interaction energy are responsible for the formation of these peculiar domain walls. Further analysis also shows that the combined parameter $J/(Z^2/\varepsilon_r a_0)$ is critical in determining the inclination of the sawtooth-shaped domain walls and its value has to satisfy certain conditions for this unique type of domain walls to appear in ferroelectrics.

This work is financially supported by the National Natural Science Foundation of China (Grants No. 11974268, No. 11574246, No. U1537210, and No. 51671194), National Basic Research Program of China (Grants No. 2015CB654903 and No. 2014CB921002), and the Key Research Program of Frontier Sciences CAS (QYZDJ-SSW-JSC010). L.W. acknowledges the support of the 2019 CAST Innovation Foundation of China. D.W. also acknowledges the support from China Scholarship Council (201706285020). L.B. acknowledges ONR Grant No. N00014-17-1-2818.

[1] W. J. Merz, Domain formation and domain wall motions in ferroelectric $BaTiO_3$ single crystals, Phys. Rev. **95**, 690 (1954).

[2] S. Wada, K. Yako, H. Kakemoto, T. Tsurumi, and T. Kiguchi, Enhanced piezoelectric properties of barium titanate single crystals with different engineered-domain sizes, J. Appl. Phys. **98**, 014109 (2005).

[3] K. Yako, H. Kakemoto, T. Tsurumi, and S. Wada, Domain size dependence of d_{33} piezoelectric properties for barium titanate single crystals with engineered domain configurations, Mater. Sci. Eng. B **120**, 181 (2005).

[4] H. J. Lee, S. J. Zhang, J. Luo, F. Li, and T. R. Shrout, Thickness-dependent properties of relaxor-$PbTiO_3$ ferroelectrics for ultrasonic transducers, Adv. Funct. Mater. **20**, 3154 (2010).

[5] D. B. Lin, S. J. Zhang, Z. R. Li, F. Li, Z. Xu, S. Wada, and T. R. Shrout, Domain size engineering in tetragonal $Pb(In_{1/2}Nb_{1/2})O_3$-$Pb(Mg_{1/3}Nb_{2/3})O_3$-$PbTiO_3$ crystals, J. Appl. Phys. **110**, 084110 (2011).

[6] E. A. Little, Dynamic behavior of domain walls in barium titanate, Phys. Rev. **98**, 978 (1955).

[7] C. T. Nelson, P. Gao, J. R. Jokisaari, C. Heikes, C. Adamo, A. Melville, S. H. Baek, C. M. Folkman, B. Winchester, Y. Gu, Y. Liu, K. Zhang, E. Wang, J. Li, L.-Q. Chen, C.-B. Eom, D. G. Schlom, and X. Pan, Domain dynamics during ferroelectric switching, Science **334**, 968 (2011).

[8] M. Dawber, K. M. Rabe, and J. F. Scott, Physics of thin-film ferroelectric oxides, Rev. Mod. Phys. **77**, 1083 (2005).

[9] P. Gao, J. Britson, J. R. Jokisaari, C. T. Nelson, S. H. Baek, Y. Wang, C. B. Eom, L. Chen, and X. Panet, Atomic-scale mechanisms of ferroelastic domain-wall-mediated ferroelectric switching, Nat. Commun. **4**, 2791 (2013).

[10] Y. M. Jin, Y. U. Wang, A. G. Khachaturyan, J. F. Li, and D. Viehland, Conformal Miniaturization of Domains with Low Domain-Wall Energy: Monoclinic Ferroelectric States Near the Morphotropic Phase Boundaries, Phys. Rev. Lett. **91**, 197601 (2003).

[11] W. S. Chang, L. C. Lim, P. Yang, C. M. Hsieh, and C. S. Tu, Rhombohedral and tetragonal nanotwin domains and thermally induced phase transformations in PZN-8%PT single crystals, J. Phys.: Condens. Matter **20**, 445218 (2008).

[12] A. Roelofs, N. A. Pertsev, R. Waser, F. Schlaphof, L. M. Eng, C. Ganpule, V. Nagarajan, and R. Ramesh, Depolarizing-field-mediated 180° switching in ferroelectric thin films with 90° domains, Appl. Phys. Lett. **80**, 1424 (2001).

[13] D. J. Jung, M. Dawber, J. F. Scott, L. J. Sinnamon, and J. M. Gregg, Switching dynamics in ferroelectric thin films: An experimental survey, Integrat. Ferroelectr. **48**, 59 (2002).

[14] R. Gysel, I. Stolichnov, N. Setter, and M. Pavius, Ferroelectric film switching via oblique domain growth observed by cross-sectional nanoscale imaging, Appl. Phys. Lett. **89**, 082906 (2006).

[15] S. Prosandeev, B. Xu, and L. Bellaiche, Polarization switching in the $PbMg_{1/3}Nb_{2/3}O_3$ relaxor ferroelectric: An atomistic effective Hamiltonian study, Phys. Rev. B **98**, 024105 (2018).

[16] S. Boyn, J. Grollier, G. Lecerf, B. Xu, N. Locatelli, S. Fusil, S. Girod, C. Carrétéro, K. Garcia, S. Xavier, J. Tomas, L. Bellaiche, M. Bibes, A. Barthélémy, S. Saighi, and V. Garcia, Learning through ferroelectric domain dynamics in solid-state synapses, Nat. Commun. **8**, 14736 (2017).

[17] B. Xu, V. Garcia, S. Fusil, M. Bibes, and L. Bellaiche, Intrinsic polarization switching mechanisms in BiFeO, Phys. Rev. B **95**, 104104 (2017).

[18] H. Wang, J. Zhu, N. Lu, A. A. Bokov, Z.-G. Ye, X. W. Zhang, Hierarchical micro/nanoscale domain structure in M_C phase of $(1-x)Pb(Mg_{1/3}Nb_{2/3})O_3$-$xPbTiO_3$ single crystal, Appl. Phys. Lett. **89**, 042908 (2006).

[19] F. Bai, J. Li, and D. Viehland, Domain hierarchy in annealed (001)-oriented $Pb(Mg_{1/3}Nb_{2/3})O_3$-$xPbTiO_3$ single crystals, Appl. Phys. Lett. **85**, 2313 (2004).

[20] G. Xu, J. Wen, C. Stock, and P. M. Gehring, Phase instability induced by polar nanoregions in a relaxor ferroelectric system, Nat. Mater. **7**, 562 (2008).

[21] M. F. Wong and K. Zeng, Nanoscale domains and preferred cracking planes in $Pb(Zn_{1/3}Nb_{2/3})O_3$–(6–7)% $PbTiO_3$ single

crystals studied by piezoresponse force microscopy and fractography, J. Appl. Phys. **107**, 124104 (2010).

[22] A. Al-Barakaty, S. Prosandeev, D. Wang, B. Dkhil, and L. Bellaiche, Finite-temperature properties of the relaxor $PbMg_{1/3}Nb_{2/3}O_3$ from atomistic simulations, Phys. Rev. B **91**, 214117 (2015).

[23] A. R. Akbarzadeh, S. Prosandeev, E. J. Walter, A. Al-Barakaty, and L. Bellaiche, Finite-Temperature Properties of $Ba(Zr, Ti)O_3$ Relaxors From First Principles, Phys. Rev. Lett **108**, 257601 (2012).

[24] P. S. Bednyakov, B. I. Sturman, T. Sluka, A. K. Tagantsev, and P. V. Yudin, Physics and applications of charged domain walls, npj Comput. Mater. **4**, 65 (2018).

[25] P. S. Bednyakov, T. Sluka, A. K. Tagantsev, D. Damjanovic, and N. Setter, Formation of charged ferroelectric domain walls with controlled periodicity, Sci. Rep. **5**, 15819 (2015).

[26] Y. L. Li, S. Y. Hu, and L. Q. Chen, Ferroelectric domain morphologies of (001) $Pb(Zr_{1-x}, Ti_x)O_3$ epitaxial thin films, J. Appl. Phys. **97**, 034112 (2005).

[27] C.-L. Jia, L. Jin, D. Wang, S. B. Mi, M. Alexe, D. Hesse, H. Reichlova, X. Marti, L. Bellaichef, and K. W. Urbana, Nanodomains and nanometer-scale disorder in multiferroic bismuth ferrite single crystals, Acta Mater. **82**, 356 (2015).

[28] Y.-H. Chu, L. W. Martin, M. B. Holcomb, and R. Ramesh, Controlling magnetism with multiferroics, Mater. Today **10**, 16 (2007).

[29] J. Wang, J. B. Neaton, H. Zheng, V. Nagarajan, S. B. Ogale, B. Liu, D. Viehland, V. Vaithyanathan, D. G. Schlom, U. V. Waghmare, N. A. Spaldin, K. M. Rabe, M. Wuttig, and R. Ramesh, Epitaxial $BiFeO_3$ mutiferroic thin film heterostructures, Science **299**, 1719 (2003).

[30] J. R. Teague, R. Gerson, and W. J. James, Dielectric hysteresis in single crystal $BiFeO_3$, Solid State Commun. **8**, 1073 (1970).

[31] D. Wang, J. Weerasinghe, and L. Bellaiche, Atomistic Molecular Dynamic Simulations of Multiferroics, Phys. Rev. Lett **109**, 067203 (2012).

[32] M. Zou, Y. Tang, Y. Feng, Y. Zhu, and X. Ma, Ferroelectric thin films in the 180° charged domain wall of the scale structure features, J. Chin. Electr. Microsc. Soc. **37**, 468 (2018).

[33] N. Curland and D. E. Speljotis, Transition region in recorded magnetization patterns, J. Appl. Phys. **41**, 1099 (1970).

[34] K. Moon, J. Cho, C. Kim, J. Yoon, D. Kim, K. Song, B. Chun, D. Kim, and C. Hwang, Triangular and Sawtooth Magnetic Domains in Measuring the Dzyaloshinskii-Moriya Interaction, Phys. Rev. Appl. **10**, 064014 (2018).

[35] The estimated value of 1.64 $|e_0|$ is obtained using $\rho^{\text{bound}} = -\nabla \cdot \boldsymbol{P}$, assuming $|\boldsymbol{P}| = 95\ \mu C/cm^2$ and $BiFeO_3$'s lattice constant. The value (1.16 $|e_0|$) used in the MC simulations is obtained by considering the parameters used in the effective Hamiltonian for $BiFeO_3$ [31] and the local mode value numerically obtained at 300 K.

[36] J. Seidel, L. W. Martin, Q. He, Q. Zhan, Y.-H. Chu, A. Rother, M. E. Hawkridge, P. Maksymovych, P. Yu, M. Gajek, N. Balke, S. V. Kalinin, S. Gemming, F. Wang, G. Catalan, J. F. Scott, N. A. Spaldin, J. Orenstein, and R. Ramesh, Conduction at domain walls in oxide multiferroics, Nat. Mater. **8**, 229 (2009).

[37] L. J. McGilly, C. S. Sandu, L. Feigl, D. Damjanovic, and N. Setter, Nanoscale defect engineering and the resulting effects on domain wall dynamics in ferroelectric thin films, Adv. Funct. Mater. **27**, 1605196 (2017).

[38] P. Sharma, D. Sando, Q. Zhang, X. Cheng, S. Prosandeev, R. Bulanadi, S. Prokhorenko, L. Bellaiche, L. Q. Chen, V. Nagarajan, and J. Seidel, Conformational domain wall switch, Adv. Funct. Mater. **29**, 1807523 (2019).

[39] T. Sluka, P. Mokry, and N. Setter, Static negative capacitance of a ferroelectric nano-domain nucleus, Appl. Phys. Lett. **111**, 152902 (2017).

[40] I. Luk'yanchuk, Y. Tikhonov, A. Sené, A. Razumnaya, and V. M. Vinokur, Harnessing ferroelectric domains for negative capacitance, Commun. Phys. **2**, 22 (2019).

[41] B. M. Vul, G. M. Guro, and I. I. Ivanchik, Encountering domains in ferroelectrics, Ferroelectrics **6**, 29 (1973).

[42] T. Sluka, A. K. Tagantsev, P. Bednyakov, and Nava Setter, Free-electron gas at charged domain walls in insulating $BaTiO_3$, Nat. Commun. **4**, 1808 (2013).

[43] T. Rojac, A. Bencan, G. Drazic, N. Sakamoto, H. Ursic, B. Jancar, G. Tavcar, M. Makarovic, J. Walker, B. Malic, and D. Damjanovic, Domain-wall conduction in ferroelectric $BiFeO_3$ controlled by accumulation of charged defects, Nat. Mater. **16**, 322 (2017).

[44] T. Sluka, A. K. Tagantsev, D. Damjanovic, M. Gureev, and N. Setter, Enhanced electromechanical response of ferroelectrics due to charged domain walls, Nat. Commun. **3**, 748 (2012).

[45] L. Li, P. Gao, C. T. Nelson, J. R. Jokisaari, Y. Zhang, S.-J. Kim, A. Melville, C. Adamo, D. G. Schlom, and X. Pan, Atomic scale structure changes induced by charged domain walls in ferroelectric materials, Nano Lett. **13**, 5218 (2013).

[46] V. Ya. Shur, E. L. Rumyantsev, E. V. Nikolaeva, and E. I. Shishkin, Formation and evolution of charged domain walls in congruent lithium niobate, Appl. Phys. Lett. **77**, 3636 (2000).

[47] P. Mokrý, A. K. Tagantsev, and J. Fousek, Pressure on charged domain walls and additional imprint mechanism in ferroelectrics, Phys. Rev. B **75**, 094110 (2007).

[48] M. Y. Gureev, P. Mokry, A. K. Tagantsev, and N. Setter, Ferroelectric charged domain walls in an applied electric field, Phys. Rev. B **86**, 104104 (2012).

[49] R. G. McQuaid, Domain patterns and domain wall dynamics in small-scale ferroelectrics, Doctoral thesis, Queen's University Belfast, 2012.

[50] A. A. Esin, D. O. Alikin, A. P. Turygin, A. S. Abramov, J. Hrescak, J. Walker, T. Rojac, A. Bencan, B. Malic, A. L. Kholkin, and V. Ya. Shur, Dielectric relaxation and charged domain walls in $(K,Na)NbO_3$-based ferroelectric ceramics, J. Appl. Phys. **121**, 074101 (2017).

[51] W. Zhong, D. Vanderbilt, and K. M. Rabe, First-principles theory of ferroelectric phase transitions for perovskites: The case of $BaTiO_3$, Phys. Rev. B **52**, 6301 (1995).

[52] S. Prosandeev, D. Wang, A. R. Akbarzadeh, and L. Bellaiche, First-principles-based effective Hamiltonian simulations of bulks and films made of lead-free $Ba(Zr,Ti)O_3$ relaxor ferroelectrics, J. Phys.: Condens. Matter **27**, 223202 (2015).

[53] D. Wang, J. Weerasinghe, A. Albarakati, and L. Bellaiche, Terahertz dielectric response and coupled dynamics of ferroelectrics and multiferroics from effective Hamiltonian simulations, Int. J. Mod. Phys. B **27**, 1330016 (2013).

[54] H. Ye, D. Wang, Z. Jiang, S. Cheng, and X. Wei, Ferroelectric phase transition of perovskite $SnTiO_3$ based on the first principles, Acta Phys. Sinica **65**, 237101 (2016).

[55] D. Wang, J. Hlinka, A. A. Bokov, Z. G. Ye, P. Ondrejkovic, J. Petzelt, and L. Bellaiche, Fano resonance and dipolar relaxation in lead-free relaxors, Nat. Commun. **5**, 5100 (2014).

[56] D. Wang, A. A. Bokov, Z. G. Ye, J. Hlinka, and L. Bellaiche, Subterahertz dielectric relaxation in lead-free $Ba(Zr,Ti)O_3$ relaxor ferroelectrics, Nat. Commun. **7**, 11014 (2016).

[57] See Supplemental Material at http://link.aps.org/supplemental/10.1103/PhysRevB.101.060103 for results from the more sophisticated phenomenological model and additional discussion.

[58] It shall be noted that ε_r is directly taken from the effective Hamiltonian [51,60]. On the other hand, in the effective Hamiltonian, the short-range interactions are kept to the third nearest neighbors described by seven parameters (j_1 to j_7; see Fig. 1 of Ref. [51]). Here in the minimal model, their effects are summarized in a single parameter J.

[59] D. Albrecht, S. Lisenkov, W. Ren, D. Rahmedov, I. A. Kornev, and L. Bellaiche, Ferromagnetism in multiferroic $BiFeO_3$ films: A first-principles-based study, Phys. Rev. B **81**, 140401(R) (2010).

[60] I. A. Kornev, S. Lisenkov, R. Haumont, B. Dkhil, and L. Bellaiche, Finite-Temperature Properties of Multiferroic $BiFeO_3$, Phys. Rev. Lett **99**, 227602 (2007).

[61] O. Dieguez, P. Aguado-Puente, J. Junquera, and J. Ĩniguez, Domain walls in a perovskite oxide with two primary structural order parameters: First-principles study of $BiFeO_3$, Phys. Rev. B **87**, 024102 (2013).

[62] Y. Wang, C. Nelson, A. Melville, B. Winchester, S. Shang, Z.-K. Liu, D. Schlom, X. Pan, and L.-Q Chen, $BiFeO_3$ Domain Wall Energies and Structures: A Combined Experimental and Density Functional Theory + U study, Phys. Rev. Lett. **110**, 267601 (2013).

[63] Y. X. Jiang, Y. J. Wang, D. Chen, Y. L. Zhu, and X. L. Ma, First-principles study of charged steps on 180° domain walls in ferroelectric $PbTiO_3$, J. Appl. Phys. **122**, 054101 (2017).

[64] D. Wang, J. Liu, J. Zhang, S. Raza, X. Chen, and C.-L. Jia, Ewald summation for ferroelectric perovksites with charges and dipoles, Comput. Mater. Sci. **162**, 314 (2019).

[65] A. Santos, M. Girotto, and Y. Levin. Simulations of Coulomb systems with slab geometry using an efficient 3D Ewald summation method, J. Chem. Phys. **144**, 144103 (2016).

[66] Y. Li, S. Hu, Z. Liu, and L. Chen, Effect of substrate constraint on the stability and evolution of ferroelectric domain structures in thin films, Acta Mater. **50**, 395 (2002).

[67] Y. Wang, Y. Zhu, and X. L. Ma, Chiral phase transition at 180° domain walls in ferroelectric $PbTiO_3$ driven by epitaxial compressive strains, J. Appl. Phys. **122**, 134104 (2017).

[68] S. O. Kasap, *Principles of Electronic Materials and Devices* (McGraw-Hill, New York, 2006).

[69] L. Chen, C. Paillard, H. Zhao, J. Íñiguez, Y. Yang, and L. Bellaiche, Tailoring properties of hybrid perovskites by domain-width engineering with charged walls, npj Comput. Mater. **4**, 75 (2018).

[70] L. Lu, Y. Nahas, M. Liu, H. Du, Z. Jiang, S. Ren, D. Wang, L. Jin, S. Prokhorenko, C.-L. Jia, and L. Bellaiche, Topological Defects with Distinct Dipole Configurations in $PbTiO_3/SrTiO_3$ Multilayer Films, Phys. Rev. Lett. **120**, 177601 (2018).

[71] H. Knüpfer and C. B. Muratov, Domain structure of bulk ferromagnetic crystals in applied fields near saturation, J. Nonlinear Sci. **21**, 921 (2011).

[72] I. A. Privorotskii, Thermodynamic theory of domain structures, Rep. Prog. Phys. **35**, 115 (2002).